A&A 365, 431–439 (2001)
DOI: 10.1051/0004-6361:20000071

Astronomy & Astrophysics

The new Basel high-latitude field star survey of the Galaxy

V. The metallicity distributions in the inner-Galaxy fields SA 107 and NGC 6171

J. Rong[1], R. Buser[2], and S. Karaali[3]

[1] Astronomy Department, Nanjing University, Nanjing 210008, China
[2] Astronomisches Institut der Universität Basel, Venusstr. 7, 4102 Binningen, Switzerland
[3] Istanbul University Science Faculty, Department of Astronomy and Space Sciences, 34452 University–Istanbul, Turkey

Received 26 July 2000 / Accepted 24 October 2000

Abstract. We discuss star count and three-color data for the two inner-Galaxy fields SA 107 and NGC 6171 observed in the new Basel *RGU* high-latitude field star survey. Our analysis is based on the structural models of the Galactic population components that were derived from the previous studies of seven fields mainly in the outer Galaxy (Buser et al. 1998, 1999, hereafter Papers I and II, respectively). Apart from the canonical structural parameters, we here explore some of the special conditions prevailing in the transition region from high to low latitudes approaching the Galactic bulge, such as interstellar reddening, preponderant sampling of giants, and possible large-scale radial metallicity gradients. We show that the data are consistent on a high confidence level with a model incorporating an old-thin disk with local mean metallicity $\langle[M/H]\rangle = -0.13 \pm 0.21$ dex at galactocentric distance $R \sim 7.3$ kpc and radial abundance gradient $\partial[M/H]/\partial x = -0.078 \pm 0.016$ dex/kpc, and a thick disk with mean metallicity $\langle[M/H]\rangle = -0.73 \pm 0.15$ dex and vertical metallicity gradient $\partial[M/H]/\partial z = -0.07 \pm 0.03$ dex/kpc. Any radial gradient of the thick disk is shown to be marginal, $0 \geq \partial[M/H]/\partial x \geq -0.02$ dex/kpc. For the inner halo, we find a gradient-less metal-weak component with mean metallicity $\langle[M/H]\rangle \sim -1.8 \pm 0.3$ dex but also evidence of a – possibly localized – metal-rich component having $\langle[M/H]\rangle = -1.0 \pm 0.2$ dex. These results provide an important further step toward a comprehensive and detailed mapping of the larger-scale density and metallicity structures of the Galaxy, to be derived from the full-survey data in 14 fields.

Key words. surveys – Galaxy: abundances – Galaxy: fundamental parameters – Galaxy: general – Galaxy: stellar content – Galaxy: structure

1. Introduction

Among all 14 fields of the new Basel survey, the two fields investigated here are distinguished by the facts that they are the only ones (i) for which non-negligible interstellar reddening has been detected within the (small) field areas, and (ii) which probe the inner Galaxy at intermediate latitude and near the transition from the halo to the bulge[1]. Because of the associated enhanced space densities and the relatively longer radial distances within the thin and thick disks sampled along the lines of sight, also relatively larger fractions of giants are being sampled in these fields for each population component. Thus, while interstellar reddening and extinction require another, complicating dimension to the exploration of parameter space, in turn the preponderance of distant giants in the star counts can be exploited for a more reliable determination of the radial density and metallicity structures of the Galaxy than has been possible from the seven higher-latitude and/or outer-Galaxy fields analysed so far in Papers I and II. The present paper thus provides another indispensable development step toward the comprehensive analysis of the full survey data in all 14 fields.

The observations and the main steps and tools of the analysis are briefly described in Sects. 2 and 3, respectively. The optimized results for the structural parameters and the metallicity distributions are presented in Sect. 4 and discussed in the concluding Sect. 5.

2. Observational data

The field data for SA 107 and NGC 6171 are summarized in Table 1. While the catalogs of photometric data are extensively described in Buser et al. (2001), here we only

Send offprint requests to: R. Buser,
e-mail: Roland.Buser@unibas.ch

[1] A general introduction to and overview of the new Basel survey is given in Paper I and in Buser & Rong (1995).

Table 1. Field data[1]

Field	l	b	Area (deg^2)	$m_{G,\mathrm{cat}}$	$m_{G,\mathrm{lim}}$	E_{G-R}[2]	No. of stars
SA 107	5.7	+41.3	0.95	17.0	16.5	0.11	532
NGC 6171	3.3	+22.8	0.92	18.5	18.0	0.40	1970

[1] The catalog of photometric data is being published in Buser et al. (2001, Paper IV).
[2] Derived in Sect. 3 below.

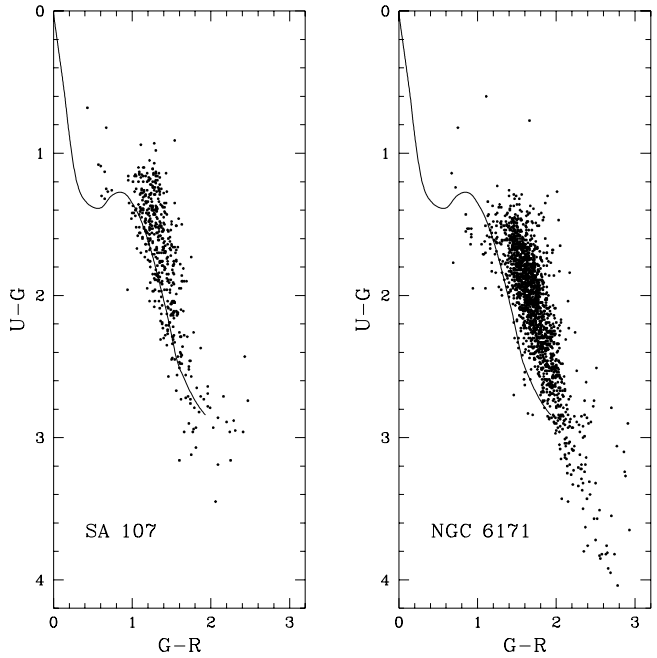

Fig. 1. The observed $(U-G, G-R)$ two-color diagrams for fields SA 107 (left) and NGC 6171 (right). The plots include all stars with apparent magnitudes down to the catalog limit $m_{G,\mathrm{cat}} = 17.0$ mag in SA 107 and to the completeness limit $m_{G,\mathrm{lim}} = 18.0$ in NGC 6171. The solid lines represent the intrinsic solar-metallicity standard main sequence

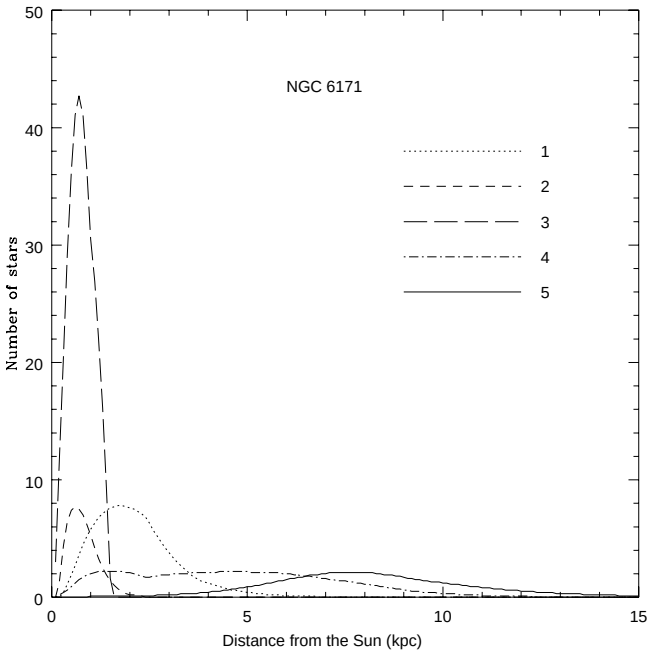

Fig. 2. Distributions of stars as functions of distance from the Sun, contributed by the different population components in field NGC 6171: (1) thin-disk giants; (2) thin-disk bright dwarfs $(M_G < 5)$; (3) thin-disk faint dwarfs $(M_G > 5)$; (4) thick disk giants; (5) halo giants. Note the extended ranges within which the giants of the different population components can be seen, and the pattern of their changing number proportions as the line of sight leaves the thin disk and penetrates into the halo

emphasize that for SA 107, the relatively bright apparent magnitude and completeness limit, $m_{G,\mathrm{lim}}$, is due to the corresponding bright magnitude limit set by the available calibration data and by the (stringent) homogeneity requirement that photographic data are strictly derived without extrapolation beyond the ranges of photoelectric and/or CCD standard-UBV sequences in all 14 program fields of the new Basel survey (Paper I). Full exploitation of the photographic measurements in this field down to the actual plate limit near $m_G \sim 19.0$ mag (Becker & Fenkart 1976; Becker & Steppe 1977) will be attempted in the future from new CCD observations of fainter standard stars.

The resulting photometry is illustrated in Fig. 1, where the stellar $U-G, G-R$ two-color distributions in the two fields are plotted along with the intrinsic standard main sequence for normal Population I (i.e., solar-abundance) stars given by Buser & Fenkart (1990). It is evident that these distributions represent mixtures of primarily old populations affected by both interstellar reddening and metallicity-induced ultraviolet excess.

3. Analysis

3.1. Tools and procedures

The tools and procedures used in the present analysis are the same as those developed in Paper I and amplified in Paper II. Briefly, for each field we calculate the star counts and color distributions (illustrated in Figs. 2 and 3) from parameterized structural models including four Galactic components which are characterized by their specific, metallicity-dependent luminosity functions and color-magnitude relations. The model parameters, mean metallicities, and metallicity gradients are allowed to vary systematically within appropriate ranges suggested by previous work (cf. Table 2), and results for a correspondingly large number of models are compared to the observed

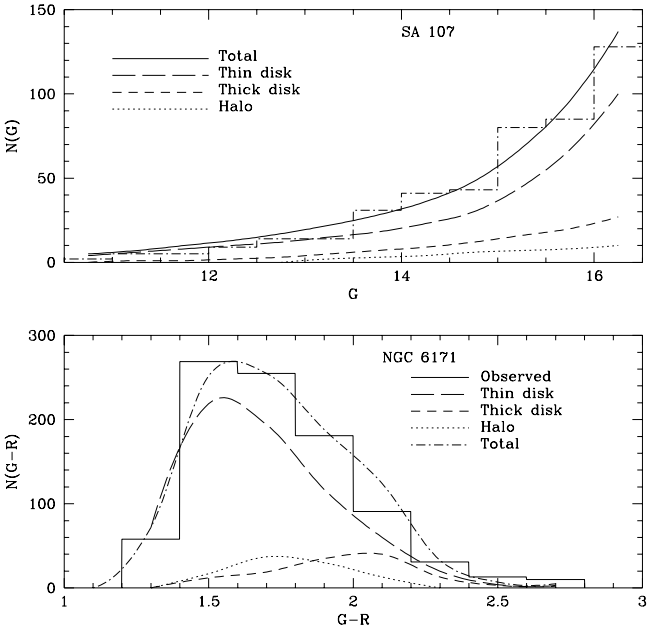

Fig. 3. Star counts $N(G)$ in the field SA 107 (upper) and color distribution $N(G-R)$ in the field NGC 6171 (lower). The observed histograms are compared with the predicted totals built up by the contributions from the individual components. The underlying structural models also include interstellar extinction according to the optimized reddening solutions derived in Sect. 3.2

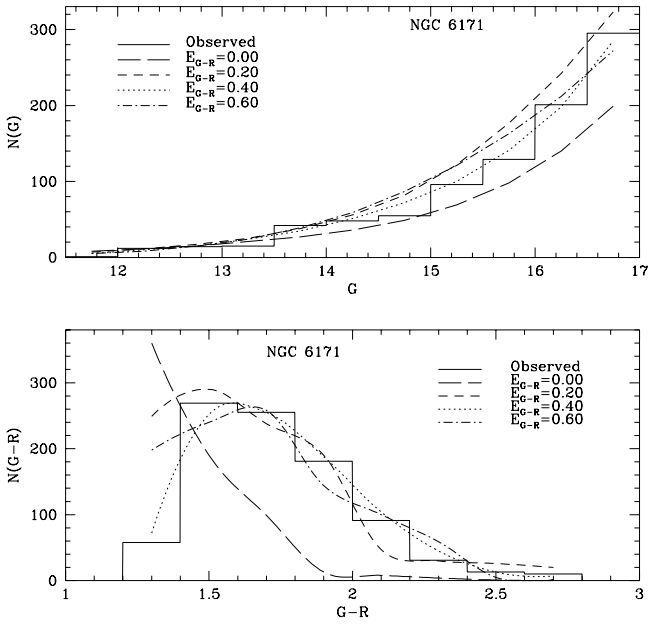

Fig. 4. Best-fitting star count (upper) and color-distribution (lower) model predictions for different assumed values of E_{G-R} and compared to observations in the field NGC 6171. Note the strong constraint imposed by the sharp observed blue cutoff at $G-R \leq 1.4$

data in each individual field. A least-squares algorithm is then used to evaluate optimum parameter values for both individual fields and their combination.

As anticipated in the introductionary Sect. 1 and detailed in the following Sect. 3.2, treatment of interstellar reddening and extinction effects has been implemented as a new element in the analysis of the fields investigated in the present paper.

3.2. Interstellar reddening and extinction

Preliminary analyses of the two-color diagrams (Fig. 1) have shown interstellar reddening to be rather uniform in either of the two fields, with large majorities of stars affected by color excesses, E_{G-R}, of order $\sim$0.15 mag (SA 107) and $\sim$0.45 mag (NGC 6171), respectively (Karaali 1998). These values are consistent with $E_{B-V} = 0.09$ mag derived for SA 107 by Burstein & Heiles (1982) and with the reddening range $0.37 \geq E_{B-V} \geq 0.18$ mag spanned by the extremes measured for the calibration cluster (NGC 6171) near the NGC 6171-field by Dickens & Roland (1972) and by Crawford & Barnes (1975).

For a more definitive assessment, here we introduce E_{G-R} as an independent additional parameter which is variable within appropriate ranges and whose optimized, field-specific values are determined from the χ^2-fits between the calculated and the observed star count and color data. The corresponding reddening in $U-G$ color and the total absorptions in the G and V magnitude bands are computed using the synthetic photometry tables providing E_{U-G}/E_{G-R}, A_G/E_{G-R}, and A_V/E_{G-R} (Buser 1978).

Figure 4 illustrates the changes in the star counts and color distribution for the field near NGC 6171 which are predicted by the best-fitting model obtained for each of the different assumed values of E_{G-R}, and the corresponding Min[χ^2]-curves for fields NGC 6171 and SA 107 are displayed in Fig. 5. Note that these curves outline the best fits to the data at *any* adopted value of E_{G-R} but including variations of *all other parameters* within their permissible ranges. Obviously then, the optimum reddening solutions are given by Min{Min[$\chi^2(p)$]}, where $p = E_{G-R}$. According to the recent all-sky model of interstellar reddening derived from comprehensive available spectral and photometric observations by Arenou et al. (1992), these solutions are consistent with foreground dust absorption screens in the Galactic thin disk out to distances r_0 from the sun of 227 pc toward SA 107 and of 302 pc toward NGC 6171. Thus, individual reddening and extinction values for the 14 (SA 107) and 42 (NGC 6171) stars predicted by the model to be lying within the dust at distances $r \leq r_0$ are then assumed to follow the empirical law $A_V = \alpha r + \beta r^2$, where the coefficients α and β are again taken from Arenou et al. (1992). For all other stars, $r \geq r_0$ and $A_G = 2.9 E_{G-R}$, where the numerical factor (2.9) is a representative mean for late-type stars (Buser 1978) and E_{G-R} is the optimal solution taken from Fig. 5.

Table 2. Adopted variation ranges of primary parameters

Component		Parameter	Symbol	Unit[1]	Range adopted
Thin disk		scale length	d_1	kpc	1.0–5.5
	old	scale height dwarfs	h_1	325 pc	0.8–1.5
	young	scale height	h_3	kpc	0.05–0.20
Thick disk		local density	n_1	n_0	0.00–0.07
		scale height	h_4	kpc	0.3–1.1
Halo		local density	n_2	n_0	0.00–0.0025

[1] $n_0 = 0.11$ stars/pc^3 is the optimized value derived in Paper II for the local density of the old thin disk.

Table 3. Optimized parameter values

	Primary parameters, $\bar{p}$						Secondary parameters, $\bar{p}$					
	Thin disk			Thick disk		Halo	Thin disk			Thick disk	Halo	
Field	d_1	h_1	h_3	n_1	h_4	n_2	n_0	h_2	d_2	d_3	$R_{\rm eff}$	κ_0
SA 107	3.72	1.17	0.15	0.047	0.81	0.00030	0.11	0.25	3.75	3.81	2.70	0.85
NGC 6171	3.66	1.18	0.11	0.034	0.85	0.00021	0.12	0.27	3.75	3.68	2.69	0.85
Combined $\bar{p}$	3.69	1.18	0.12	0.038	0.84	0.00023	0.12	0.26	3.75	3.74	2.70	0.85
Combined $\sigma_{\bar{p}}$	0.80	0.21	0.04	0.015	0.30	0.00015	0.01	0.05	1.00	1.00	–	–
Papers I $\vee$ II $\bar{p}$	4.01	0.88	0.14	0.059	0.91	0.00045	0.11	0.25	3.75	3.00	2.69	0.84
Papers I $\vee$ II $\sigma_{\bar{p}}$	1.00	0.15	0.03	0.030	0.30	0.00030	0.01	0.05	1.00	1.50	–	–

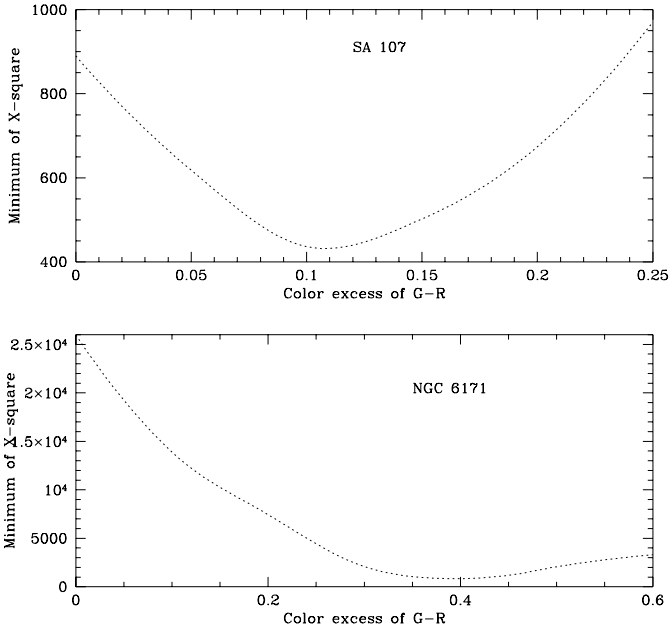

Fig. 5. Min$[\chi^2(p)]$-curves as functions of the color excess, $p = E_{G-R}$, for the two fields SA 107 and NGC 6171. Acceptable models provide optimized solutions $E_{G-R} = 0.11 \pm 0.04$ mag (upper) and $E_{G-R} = 0.40 \pm 0.05$ mag (lower), respectively, for the two fields

4. Results

4.1. Optimized structural parameters

Based on the systematic calculations of models covering the full parameter ranges adopted in Table 2, optimized values and constraints of the parameters have been derived for both the individual fields and their combination. Results are summarized in Table 3 where, for comparison, the earlier results obtained for the combined survey of seven fields in Papers I and II have been added in the two bottom lines. For each primary parameter, the two principal derivation steps are also given in terms of the Min$[\chi^2(p)]$-curve and its associated frequency distributions, $F(p, \xi)$. Representative plots of thin-disk parameters are illustrated for the field NGC 6171 in Fig. 6, while thick-disk parameters are shown for the field SA 107 in Fig. 7.

4.1.1. Thin disk

For most thin-disk parameters, the present results agree within one or two sigma(s) with those obtained from the 7-field survey analyses in Papers I and II. However, there are a few interesting details which deserve further mention. First, as anticipated in the introduction, the larger range and enhanced stellar sampling at lower Galactic latitudes provided in the field near NGC 6171 do lead to a somewhat more reliable determination of, and constraint on, the old thin disk's scale length, d_1 (Fig. 6, top panels). For the same reason, we shall be able to reliably derive a radial metallicity gradient in the (inner) thin-disk component of the Galaxy below. Secondly, compared with all (8) other fields analyzed so far – which sample the disk at larger galactocentric radii –, we find the scale heights, h_1 and h_3, of the old and the young dwarfs in the NGC 6171-field

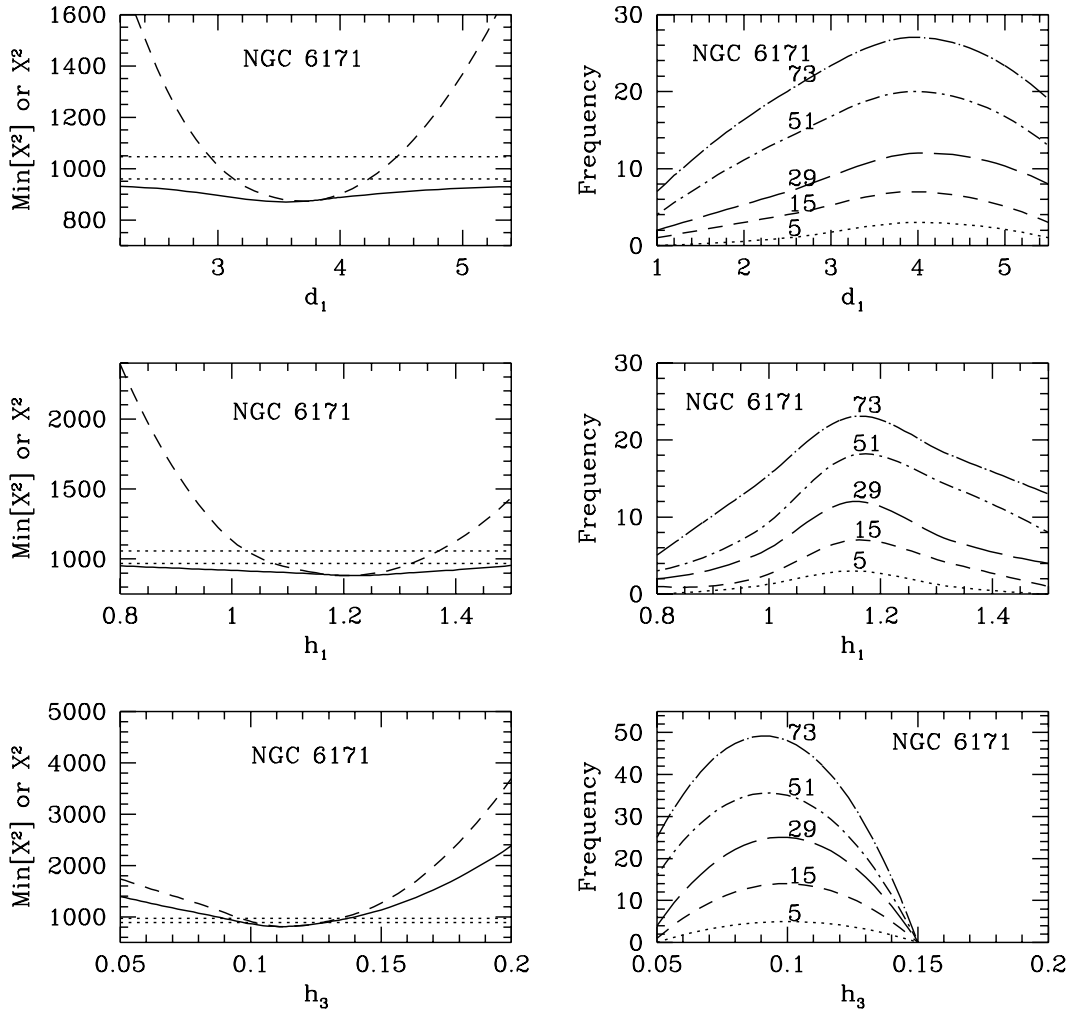

Fig. 6. Min[$\chi^2(p)$]-curves (left) and frequency distributions $F(p,\xi)$ (right) for (primary) thin-disk parameters in field NGC 6171. These parameters are, top: d_1, the scale length of the (old) thin disk; middle: h_1, the scale height parameter of the old thin-disk dwarfs – notice that the resulting optimized value $h_1 = 1.18 \pm 0.12$ corresponds to a scale height of 380 ± 40 pc; and bottom: h_3, the scale height of the young thin-disk stars. In the left-hand panels, dotted horizontal lines indicate selection limits of good models having $\chi^2_{\max}(p) \leq \xi \times \chi^2_{1,k,\min}$, where $\xi = 1.1$ and $\xi = 1.2$, respectively, and k is the field index. To illustrate the difference with the Min[χ^2]-curve (solid line), the χ^2-curve for the individual field-specific minimum has also been plotted (dashed line). In the right-hand panels, the sequence of curves from bottom to top corresponds to values of ξ growing from 1.1 to 1.5; labels indicate the number of models involved

to have the respectively largest (Fig. 6, middle panels) and smallest (Fig. 6, bottom panels) values. Qualitatively, the low(er) scale height of the young stars is consistent with (current) massive-star formation in the inner disk being confined to regions of lower thickness than in the outer Galaxy, as shown in the recent study of the radial distribution of OB star formation by Bronfman et al. (2000). On the other hand, the high scale height of the old stars supports a picture where, relative to the outer Galaxy, both star formation in and dynamical heating of the disk have set in earlier and have been going on for a longer time – and probably also more efficiently, due to higher available gas surface density – in the inner Galaxy. Thus, apart from tracing the space distributions of the Galactic stellar population components, the present survey also appears to provide vital statistical data for the study of the large-scale star formation history in the Galaxy.

4.1.2. Thick disk and halo

In the two inner-Galaxy fields investigated here, all parameters for the thick disk and the halo are found to have optimized values which are fully compatible with the earlier results of Paper II. For a moderately strong thick disk with local density $n_1 \sim 4\%$ of the local thin-disk density (Fig. 7, top panels), a relatively low scale height $h_4 \sim$ 840 pc (Fig. 7, middle panels) is confirmed, while the slightly improved value for the scale length turns out to be also slightly larger ($d_3 = 3.74 \pm 1.00$ kpc) than measured from the 7-field survey analysed in Paper II. Finally, the halo sampled in the SA 107 and NGC 6171 fields is only weak, with local density normalization $n_2 = 0.00023 \pm 0.00015$ (Fig. 7, bottom panels). As we shall see below, this result may be partly due to stronger overlaps of the stellar density and metallicity distributions of the

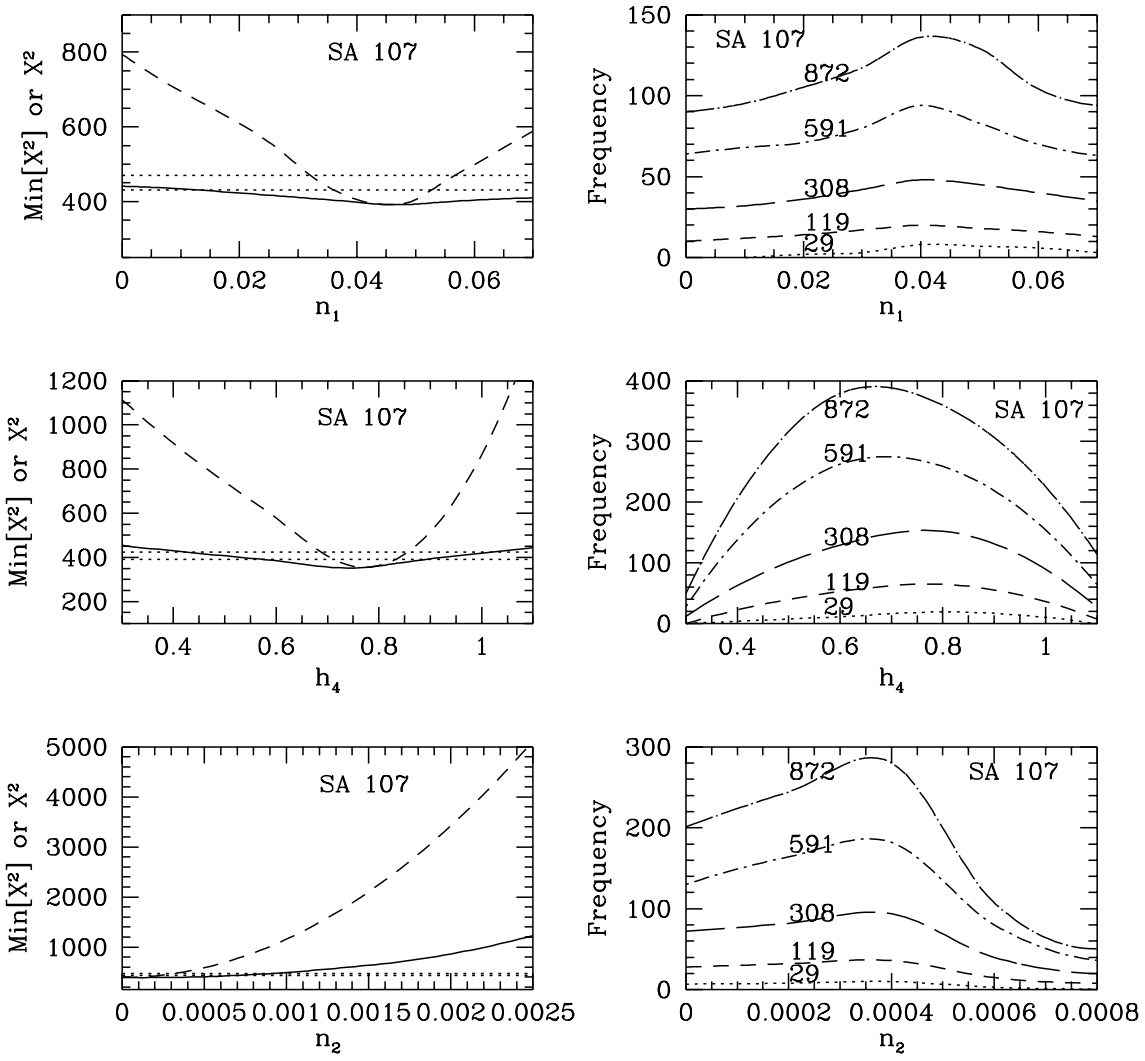

Fig. 7. Same as Fig. 6, but now for (primary) thick-disk and halo parameters in field SA 107. Top panels: n_1, the local density normalization of the thick disk; middle panels: h_4, the scale height of the thick disk; and bottom panels: n_2, the local density normalization of the halo

inner halo and thick disk – most notably in the low-latitude transition region near the NGC 6171 field – and to the resulting enhanced ambiguity in gauging the proper number proportions among these components by fitting the available data.

However in summary, the present analysis shows that the optimized structural model designed in Papers I and II also successfully accommodates the data in fields with more special characteristics, such as interstellar reddening and enhanced stellar space density and population mix in the inner Galaxy.

4.2. Mean metallicities and metallicity gradients

Mean metallicities and both radial and vertical metallicity gradients for all population components have been included as variables in the present model calculations, using the same prescriptions as encoded in Papers I and II. The most convincing proof of the reliability of the calibration, of the high degree of homogeneity, and of the useful metallicity sensitivity of the data has been provided by the unambiguous χ^2-solution for the radial gradient, shown in Fig. 8, of the thin disk in the low-latitude ($b = +22.8$ deg) field near NGC 6171. The optimized result of $\partial[M/H]/\partial x = -0.078 \pm 0.016$ dex/kpc is in excellent agreement with independent determinations based on a variety of tracer objects and methods summarized by Henry & Worthey (1999), and thus fully recovers the canonical literature value.

On the other hand, Fig. 9 shows that in both directions sampled in the present data, the thick disk component has mean metallicity $\langle[M/H]\rangle \sim -0.73$ dex but only a marginally small radial gradient, if any – constrained to $0 \geq \partial[M/H]/\partial x \geq -0.02$ dex/kpc by the NGC 6171-field data. While a zero radial gradient could be expected almost a priori for SA 107 – which due to its intermediate latitude ($b = +41.3$ deg) provides only much poorer sampling of the radial direction –,

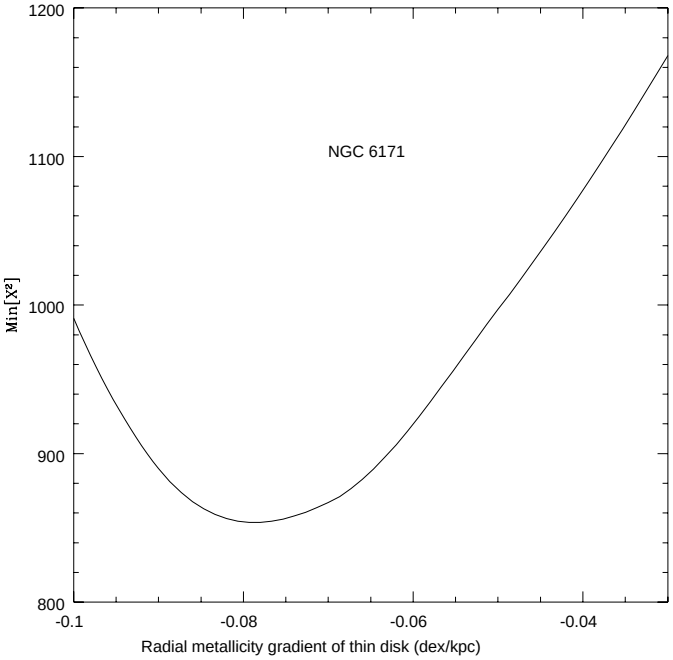

Fig. 8. Min[χ^2]-curve for the radial metallicity gradient of the thin disk as seen in field NGC 6171. The resulting optimized value is $\partial[M/H]/\partial x = -0.078 \pm 0.016$ dex/kpc, with $[M/H] = -0.23$ dex near the Sun and $\langle[M/H]\rangle = -0.13 \pm 0.21$ dex for the full thin-disk sample in this field

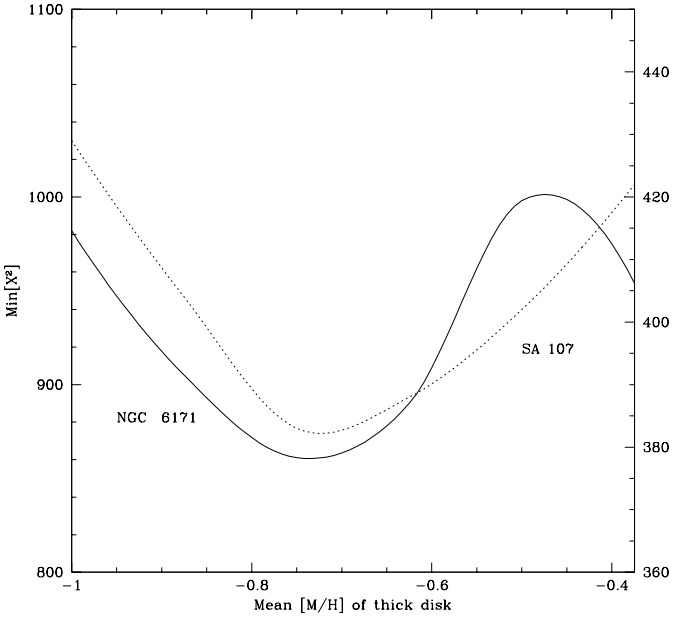

Fig. 9. Min[χ^2]-curves as functions of mean thick-disk metallicity, as seen in fields NGC 6171 (solid line) and SA 107 (dotted line). For NGC 6171, the resulting optimized model has $\langle[M/H]\rangle = -0.73 \pm 0.15$ dex but is also consistent with a radial gradient $0 \geq \partial[M/H]/\partial x \geq -0.02$ dex/kpc. For all models with stronger gradients, Min[χ^2] increases everywhere beyond acceptable values. – On the other hand, for SA107 the resulting optimized model has $\langle[M/H]\rangle = -0.73 \pm 0.25$ dex and a vertical metallicity gradient $\partial[M/H]/\partial z = -0.07 \pm 0.03$ dex/kpc

the optimized solution for this field includes a significant vertical gradient of $\partial[M/H]/\partial z = -0.07 \pm 0.03$ dex/kpc (leading to the larger derived dispersion of the mean metallicity, $\sigma_{\langle[M/H]\rangle} = 0.25$).

For the halo, a canonical (e.g., Beers & Sommer-Larsen 1995) mean metallicity $\langle[M/H]\rangle = -1.8 \pm 0.2$ dex clearly results from the SA 107 data, but appears only weakly pronounced in the direction closer to the Galactic bulge, toward NGC 6171 (Fig. 10). While systematic radial gradients $\partial[M/H]/\partial R$ in the halo can not be detected in the data in either of these two fields, the strong minimum of the Min[χ^2]-curve for NGC 6171 in Fig. 10 yields an optimized value of $\langle[M/H]\rangle = -1.0 \pm 0.2$ dex for the mean halo metallicity seen at low latitude.

Taken at face value, these results would argue in favor of the possibility that, rather than featuring a uniform large-scale profile (characterizable by well-behaved mean metallicity and dispersion and/or spatial gradients), the metallicity structure of the inner halo may be bimodal – or even multi-modal, with localized volumes having separate discrete metallicity distributions which are reminiscent of the nonuniform chemical structure observed in the outer halo (e.g., Carney 2000; Bland-Hawthorne & Freeman 2000). However, such a conclusion would be premature, because the data behind it are still limited at the present stage of this project. Furthermore, we believe a more likely interpretation of the result in Fig. 10 is that the strong signal of a high-metallicity halo component in the NGC 6171-field still suffers from contamination by thick-disk stars at $z \sim$2–3 kpc. Figure 2 shows that the thick disk and the halo provide comparable count contributions there, and these may not have been properly distinguished on account of their photometric properties, since at intermediate metallicities, the resolution of the available calibration grid is probably still too coarse for adequately modelling the strongly overlapping tails of the metallicity distributions of these two components. On the other hand, it is safe to conclude that the secondary minimum at $\langle[M/H]\rangle = -1.8$ dex in Fig. 10 represents a pure halo sample at distances $>\sim 8$ kpc from the Sun.

5. Discussion and conclusion

χ^2-tests of significance show that the results reported in the previous section define overall models of the large-scale Galaxy which are acceptable as parent populations of the data (Table 4).

It is evident that the fits to the data are still good even if the models are perturbed, i.e., if any one of the parameters is allowed to deviate from its optimized value by one sigma. Even more importantly, Table 4 also demonstrates that the differences between optimized parameter values

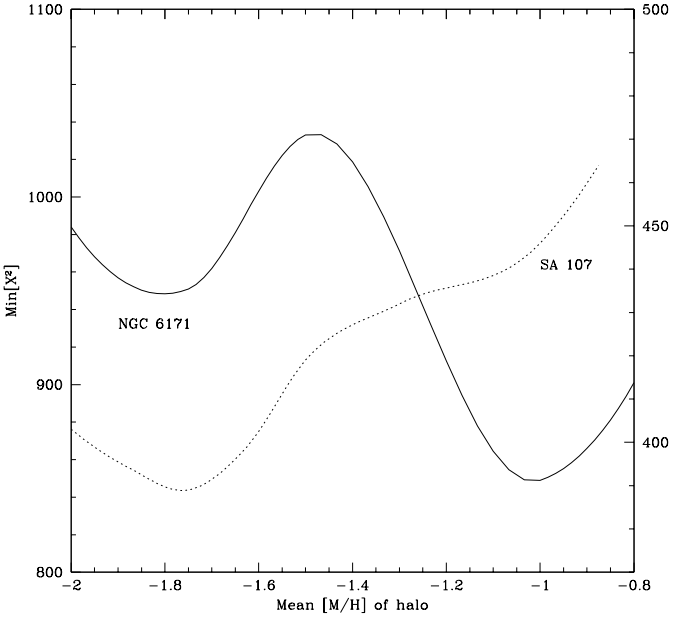

Fig. 10. Min[χ^2]-curves for uniform mean metallicity of the halo, as seen in fields NGC 6171 (solid line) and SA 107 (dotted line). For NGC 6171, the optimized model has a high mean metallicity $\langle[M/H]\rangle = -1.0 \pm 0.25$ dex, but the secondary minimum is still significant – although at a lower confidence level –, indicating that a more canonical metal-poor halo component with $\langle[M/H]\rangle = -1.8$ dex has been sampled in this field as well. Although these results show that there may be large-scale structure in the metallicity distribution of the halo, note that all models including a *radial* gradient, $\partial[M/H]/\partial R$, invariably provide Min[χ^2] scores far above the acceptance threshold, $\xi = 1.2$ (see the text). – While the minimum near $\langle[M/H]\rangle = -1.8$ dex stands out prominently in SA 107, note the absence in this field of the strong feature near $\langle[M/H]\rangle = -1$ dex seen to dominate the halo metallicity profile of the lower-latitude field NGC 6171

in the two fields (which are measured by the $\sigma_{\bar{p}}$ of the combined survey in Table 3) are highly significant, too. This result supports our earlier, preliminary conclusions of Table 5 in Paper II, viz, that the similarly large dispersions in mean thick-disk parameters determined from data in seven fields may actually be indicative of significant nonuniformity in the density and metallicity structure of the Galaxy rather than due to random fluctuations in the data.

Figure 11 is a preliminary, qualitative synopsis obtained from all 9 fields investigated up to now. It shows how the present results extend the sample range to a scale of ∼3 kpc and thus will eventually allow a more reliable determination of the radial metallicity structures in the Galaxy. In the lower part of the diagram, the mean thin-disk metallicity derived from the seven-field higher-latitude survey in Papers I and II is seen to fit reasonably well with the mean and gradient observed in the NGC 6171-field. Note that in calculating the local mean near the solar circle ($\langle X\rangle \sim 8.6$ kpc) from the individual fields, provisional vertical gradients of the thin disk, $-0.3 \geq \partial[M/H]/\partial z \geq -0.6$ dex/kpc, have been used as

Table 4. χ^2-test results

Field	Degrees of freedom	Model	Goodness of fit
SA 107	126	optimized	0.82
		perturbed	>0.70
NGC 6171	82	optimized	0.46
		perturbed	>0.31
Combined	214	optimized	0.54
		perturbed	>0.42

determined in Paper I. As these will be reevaluated on account of improved calibrations set up in the meantime (Paper II and Buser et al. 2000), we can expect to obtain an even better fit from the expanded full-survey field sample in a future paper.

The upper part of Fig. 11 shows the maximum radial gradient derived for the thick disk in Fig. 9 ($\partial[M/H]/\partial\langle X\rangle = -0.02$ dex/kpc, short-dashed line). For comparison, we also plot the maximum radial gradient emerging from the analysis of seven individual fields in Paper II ($\partial[M/H]/\partial\langle X\rangle = -0.04$ dex/kpc, long-dashed line). Note that this calculation also includes the optimized χ^2-solutions for the mean metallicity and vertical gradient in each field. Thus for completeness, these individual-field data are displayed here (solid circles) as functions of (approximate) mean projected galactocentric distance $\langle X\rangle = 8.6 \pm h_4/\tan b$ kpc, where h_4 is the (optimized) scale height of the thick disk and b is the Galactic latitude of the field[2]. Finally, open circles illustrate nonoptimized χ^2-solutions which are based on zero assumed vertical gradients and which are still consistent with the data on the three- to four-sigma level (Paper I).

There are two main conclusions that can be drawn from this amplification of our picture of the thick-disk metallicity structure provided by the new data in the NGC 6171 and SA 107 fields. First, if there is a nonzero radial gradient in this component at all, it must be rather small; and secondly, a nonzero vertical gradient, of order ∼−0.10 dex/kpc, is now strongly indicated. Taken together with the excellent reproduction of the radial gradient of the thin disk – the present results also clear much of the way on which to proceed toward the analysis of 5 remaining fields of the new Basel survey.

[2] Note that for the present, qualitative rather than quantitative, discussion we take advantage of the fact that most Basel fields are approximately arranged in a meridional cross section perpendicular to the Galactic plane and going through the Galactic center and the Sun.

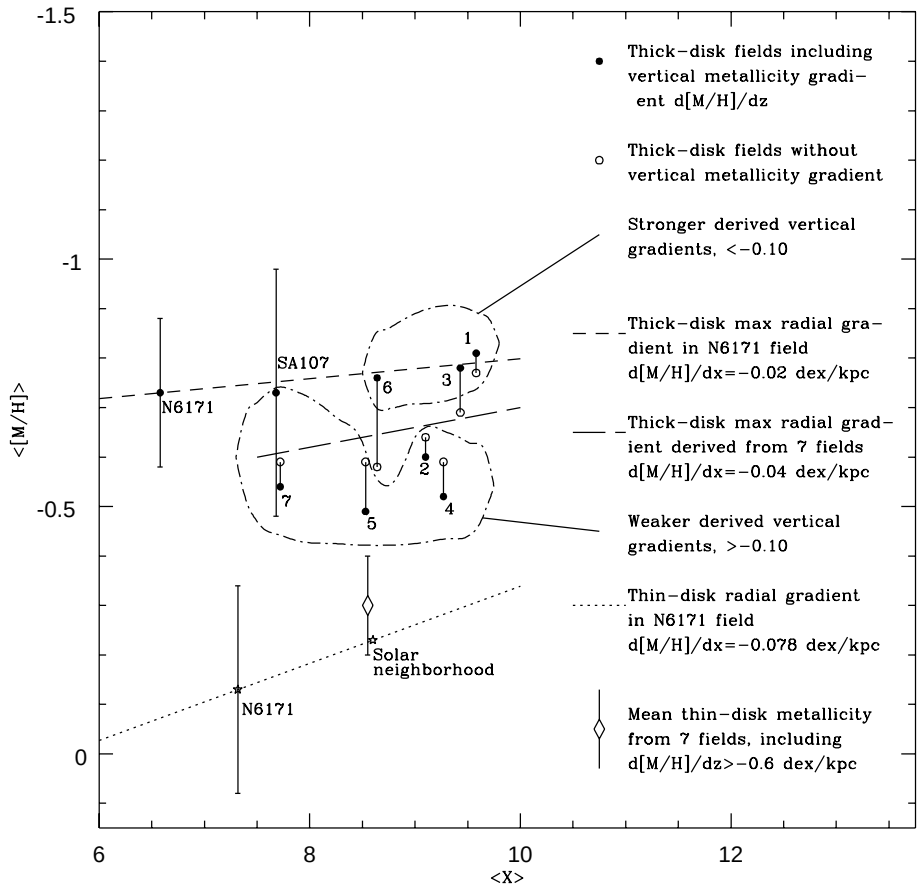

Fig. 11. Summary of metallicity structures of the Galactic thin and thick disks, as derived from the data in 9 high- and intermediate-latitude fields. Mean metallicities $\langle[M/H]\rangle$ for individual fields (circles and asterisks) and for the 7-field survey (diamond) are plotted as functions of the sampled population component's mean projected galactocentric distance $\langle X\rangle$. They are compared with the radial gradients derived here from the NGC 6171-field data for the thick disk (short-dashed line) and the thin disk (dotted line), as well as with the maximum allowed thick-disk radial gradient found from the 7-field survey in Paper II (long-dashed line). Labels 1–7 refer to the index of fields, as given in Table 1 of Paper I

Acknowledgements. This work was supported by the Swiss National Science Foundation. J. Rong also acknowledges partial financial support by the Chinese National Natural Science Foundation (19733001).

References

Arenou, F., Grenon, M., & Gómez, A. 1992, A&A, 258, 104
Becker, W., & Fenkart, R. 1976, Photometric Catalogue for Stars in Selected Areas and Other Fields in the RGU–System (I), Astron. Inst. Univ. Basel
Becker, W., & Steppe, H. 1977, A&AS, 28, 377
Beers, T., & Sommer-Larsen, J. 1995, ApJS, 96, 175
Bland-Hawthorne, J., & Freeman K. 2000, Sci, 287, 79
Bronfman, L., Casassus, S., May, J., & Nyman, L.-A. 2000, A&A, 358, 521
Burstein, D., & Heiles, C. 1982, AJ, 87, 1165
Buser, R. 1978, A&A, 62, 425
Buser, R., & Fenkart, R. P. 1990, A&A, 239, 243
Buser, R., & Rong, J. X. 1995, Baltic Astron., 4, 1
Buser, R., Rong, J. X., & Karaali, S. 1998, A&A, 331, 934, Paper I
Buser, R., Rong, J. X., & Karaali, S. 1999, A&A, 348, 98, Paper II
Buser, R., Karaali, S., Rong, J. X., Topaktas, L., & Güngör Ak, S. 2001, A&AS, in preparation, Paper IV
Buser, R., Karatas, Y., Rong, J., Lejeune, T., Westera, P., & Güngör Ak, S. 2000, A&A, 357, 988
Carney, B. W. 2000, in Star Clusters, ed. L. Labhardt, B. Binggeli, Saas-Fee Advanced Course Lecture Notes, 28 (Berlin: Springer), in press
Dickens, R. J., & Roland, A. 1972, MNRAS, 160, 37
Henry, R. B. C., & Worthey, G. 1999, PASP, 111, 919
Karaali, S. 1998, unpublished